

Ostwald ripening and breakup characteristics of the advective Cahn-Hilliard equation: The role of free energy functionals

By M. F. P. ten Eikelder[†] AND M. A. Khanwale

Ostwald ripening, the vanishing of small droplets or bubbles that arise during breakup, poses a significant challenge in the computational modeling of a wide range of multiphase systems. This process leads locally to a loss of mass in one of the phases, even when the total mass is conserved. The numerical breakup of the model (breakup due to insufficient resolution) and the mitigation of Ostwald ripening can lead to the model showing different breakup behavior under low numerical resolutions. In this paper, within the context of the advective Cahn-Hilliard phase-field model, we explore the influence of different free energy functionals on this process through numerical simulations. Our simulations show that the Ginzburg-Landau potential leads to Ostwald ripening. This phenomenon is minimized and leads to a desirable delay in numerical breakup when adopting the Flory-Huggins potential. These findings have important implications in high-fidelity multiphase simulations, particularly in high-Reynolds number flows involving breakup.

1. Introduction

Multiphase flow is ubiquitous in various fields of science and engineering, where the interaction between different phases plays a pivotal role. Understanding and predicting these complex flow phenomena requires robust modeling and discretization techniques. Phase-field modeling and computation that utilizes thermodynamic arguments has emerged as a mature modeling technology, offering solutions to the challenges inherent in multiphase flow (Anderson *et al.* 1998; Gomez & van der Zee 2018). It addresses both physical modeling and geometrical representation through a smooth scalar phase field variable that simultaneously represents a physical quantity (e.g., a concentration) and accounts for geometrical and topological changes in the interface between the two phases. This method allows for modeling complex flow physics, including capillary effects, phase transitions, and small-scale dynamics, where arbitrary topological transitions occur. Consequently, phase-field modeling provides a significant advantage over traditional methods, which become intractable for problems involving such intricate dynamics, especially when modeling multiphysics phenomena (for example, see (Mirjalili *et al.* 2020; Roccon *et al.* 2023)).

The Cahn-Hilliard (CH) equation is a pivotal phase field model for the description of multiphase systems (Cahn & Hilliard 1958). This equation provides a robust framework for understanding phase separation and coarsening in binary mixtures by minimizing a free energy functional (Elliott & Garcke 1996). It plays a central role in the Navier-Stokes Cahn-Hilliard (NSCH) model, which describes the evolution of viscous incompressible isothermal fluid mixtures with surface tension (Abels *et al.* 2012; Lowengrub & Truskinovsky 1998; ten Eikelder *et al.* 2023). This model is popular for the simulation of a wide range of

[†] Institute for Mechanics, Computational Mechanics Group, Technical University of Darmstadt, Germany

complex fluid dynamics with multiple phases—see, e.g., Khanwale *et al.* (2020); Guo *et al.* (2022); Khanwale *et al.* (2022a); ten Eikelder & Schillinger (2024).

One of the major challenges in the simulation of multiphase systems is the persistence of small droplets/bubbles that arise during breakup events, particularly in the case of high-Reynolds number situations, as this affects the droplet size distribution, an important quantity of interest. In the existing NSCH simulations of such systems, at a given mesh resolution, larger droplets typically grow at the expense of smaller ones due to violation of boundedness and minimization of the energy functional of the partial differential equation (PDE) system, especially for the small droplets, which are typically underresolved (Yue *et al.* 2007). This leads to the eventual disappearance of such small droplets or bubbles, a process known as Ostwald ripening or coarsening (Voorhees 1985). If these droplets do not coalesce, the Ostwald-ripening effect in existing NSCH simulations is unphysical.

A commonly used functional in CH is the Ginzburg-Landau (GL) potential, which characterizes the two phases by a double-well structure (Ginzburg & Landau 1950). While effective in many scenarios, the GL potential does not inherently preserve the bounds of the phase concentration, leading to potentially unphysical numerical results. This bound violation is not due to numerical discretization; it is a feature of the GL potential for the CH phase-field model. These bound violations depend on the feature size (droplet/filament) relative to the minimum numerical resolution of the simulation. In practice, a clipping procedure pulls back the phase field to its saturation bounds to calculate mixture density and viscosity, thereby preserving realizability. However, this retraction can lead to other cascading errors. To minimize this effect, different strategies have been used in the literature [e.g., penalty fluxes (Roccon *et al.* 2023), degenerate mobilities (Dai & Du 2016; Khanwale *et al.* 2022b) and dynamic interface thickness (Khanwale *et al.* 2022b)].

In this paper, we consider the Flory-Huggins (FH) potential which is a bound-preserving free energy potential rooted in the thermodynamics of mixtures (Flory 1953). Therefore, the main objective of this paper is to study the role of the free energy functional on the Ostwald ripening within the CH framework. We perform numerical simulations of the advective CH model using GL and FH potentials and discuss their effect on the small-scale droplet/bubble stability. Our results highlight the advantages of using the FH potential in preventing unphysical Ostwald ripening.

Adopting the FH potential of course introduces several challenges for numerical simulations. As a secondary objective, we propose a numerical scheme for the mixed formulation of the CH model that permits large time steps. We refer readers to Wang *et al.* (2020); Barrett *et al.* (1999) for other methods for the CH with the FH potential, and note the paper of Chen *et al.* (2024) for the simulation of the NSCH model with the FH potential with matching densities.

2. The Cahn-Hilliard model

2.1. Governing equations and properties

Let $\Omega \subset \mathbb{R}^d$, $d = 2, 3$, be an open, connected spatial domain with boundary $\Gamma = \partial\Omega$, and the unit outward normal denotes \mathbf{n} . We consider the evolution dynamics of a binary mixture in Ω governed by the advective CH equation. The problem under consideration consists of solving the strong formulation: given the (time-dependent) vector field $\mathbf{v} = \mathbf{v}(\mathbf{x}, t) : \bar{\Omega} \times \mathcal{T} \rightarrow \mathbb{R}$, find $c = c(\mathbf{x}, t) : \bar{\Omega} \times \mathcal{T} \rightarrow [0, 1]$ such that

$$\partial_t c + \operatorname{div}(c\mathbf{v}) - \operatorname{div}(m\nabla\mu) = 0, \quad \text{in } \Omega, \quad (2.1a)$$

$$\mu - \varepsilon^{-1}w(c) + \varepsilon\Delta c = 0, \quad \text{in } \Omega, \quad (2.1b)$$

$$(m\nabla\mu) \cdot \mathbf{n} = 0, \quad \text{in } \Gamma, \quad (2.1c)$$

$$\nabla c \cdot \mathbf{n} = 0, \quad \text{in } \Gamma, \quad (2.1d)$$

with $c(\mathbf{x}, 0) = c_0(\mathbf{x})$ in Ω , where the time domain is $\mathcal{T} = (0, T)$ with $T > 0$, and where we assume $\nabla \cdot \mathbf{v}(\mathbf{x}, t) = 0$ in Ω . Here $c = c(\mathbf{x}, t)$ denotes the concentration (with physical bounds $c \in [0, 1]$) of one of the two components, $w = w(c)$ is the derivative of a local potential function $W = W(c)$ ($W'(c) = w(c)$) and μ is the chemical potential. Additionally, m denotes the concentration-dependent positive mobility quantity $m = m(c) \geq 0$, and ε is a positive constant that represents the interface width. We choose $m(c) = c_+(1 - c)_+$, where $a_+ = (a + |a|)/2$ is the positive part of $a \in \mathbb{R}$. Eq. (2.1a) describes the CH evolution dynamics, Eq. (2.1b) defines the chemical potential μ and Eqs. (2.1c, 2.1d) prescribe the homogeneous boundary conditions.

The Helmholtz free energy (Ψ) associated with the system (2.1) is

$$\Psi = \Psi(c, \nabla c) = \int_{\Omega} \psi(c, \nabla c) \, dv, \quad \psi = \frac{1}{\varepsilon}W(c) + \frac{1}{2}\varepsilon\|\nabla c\|^2, \quad (2.2)$$

where ψ is the Helmholtz free energy density, and where v is the volume element. The chemical potential in Eq. (2.1b) is defined as the Fréchet derivative of Eq. (2.2):

$$\mu = \frac{\delta\Psi}{\delta c} = \frac{\partial\psi}{\partial c} - \operatorname{div} \left(\frac{\partial\psi}{\partial\nabla c} \right). \quad (2.3)$$

Next, we observe from Eqs. (2.1a) and (2.1c) that the concentration is a globally conserved quantity, i.e., $\int c(\mathbf{x}, t) \, dv = \int c(\mathbf{x}, 0) \, dv$ for all $t \in \mathcal{T}$. Additionally, in the absence of advection, we have the energy-dissipation law:

$$\frac{d}{dt}\Psi = - \int_{\Omega} m\|\nabla\mu\|^2 \, dx \leq 0, \quad (2.4)$$

where $\|\cdot\|$ is the standard Euclidean norm.

2.2. Free energy potentials

The GL double-well potential $W(c) = G(c)$ and its derivative $w(c) = g(c)$ are defined as

$$G(c) = 4c^2(1 - c)^2, \quad g(c) = 8c(2c - 1)(c - 1). \quad (2.5)$$

The structure of the GL potential reveals the underlying problem. Even though the minima of the double-well potential $G(c)$ are at $c = \pm 1$, it is well-defined for all $c \in \mathbb{R}$. As such, it contains no mechanism to keep c within the physical bounds $[0, 1]$.

The FH potential $W(c) = F(c)$ and its derivative $w(c) = f(c)$ are defined as

$$F(c) = a_3(c \log(c) + (1 - c) \log(1 - c) + a_1c(1 - c) + a_2), \quad (2.6a)$$

$$f(c) = a_3(\log(c) - \log(1 - c) + a_1(1 - 2c)), \quad (2.6b)$$

where a_1 , a_2 and a_3 are dimensionless constants. In contrast to the GL potential, the FH potential precludes values of c outside its physical bounds. As such, the FH theory is inherently a bound-preserving theory (Elliott & Garcke 1996). In Figure 1, we visualize the free energy and its derivative $w(c) = W'(c)$ for the GL and the FH model for $s = 2$, where the parameter values are defined in Table 1. We observe that $g(c)$ is well-defined for all values of c , whereas $f(c)$ becomes unbounded near $c = \pm 1$ and thus acts as a physical

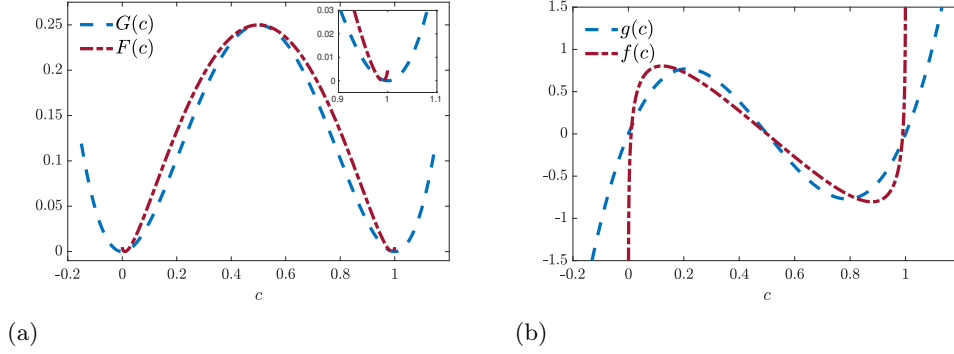


FIGURE 1. Potential $W(c)$ and its derivative $w(c) = W'(c)$ for the GL (G), and the FH potential (F). The parameter values correspond to $s = 2$; see Table 1. (a) Potentials $W(c)$, (b) Derivative of potentials $w(c)$.

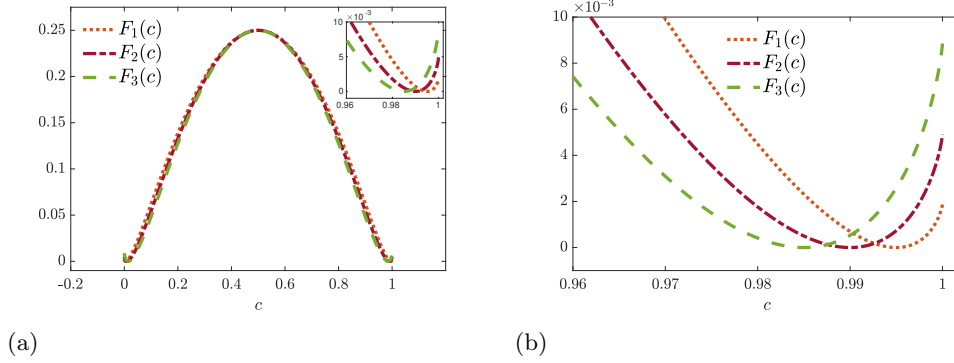


FIGURE 2. FH potentials $F(c) = F_s(c)$, for $s = 1, 2, 3$. (a) No zoom, (b) zoom.

barrier for the phase-field c to go out of bounds. Next, we note that the parameter a_1 determines the shape of the FH free energy, and, in particular, it admits a double-well shape for $a_1 > 2$ and a single-well profile for $a_1 \leq 2$. A larger a_1 shifts the minima closer to $c = 0$ and $c = 1$. The parameters in Figure 1 are selected so that the minima are near $c = 0.01$ and $c = 0.99$, where a_2 and a_3 are chosen so that $\min_c F(c) = 0$ and $\max_c F(c) = 1$. In Figure 2, we show the minima for various values of a_1 . Ideally, the value of a_1 should be chosen to be as high as numerically possible so that the saturation is close to 0 or 1. We set $c_r = c_2 - c_1$ with $c_1 < c_2$ the locations of the minima (with $c_1 + c_2 = 1$).

2.3. Nondimensionalization

We now perform the nondimensionalization of the advective CH system [Eq. (2.1)]. Introducing a characteristic length and time scales L_0 and T_0 , the units of the quantities in Eq. (2.1) are: $[c] = 1$, $[\mathbf{v}] = L_0 T_0^{-1}$, $[\mu] = L_0^{-1}$, $[\varepsilon] = L_0$, $[m] = L_0^3 T_0^{-1}$. The dimensionless variables are

$$\mathbf{x}^* = \frac{\mathbf{x}}{L_0}, \quad \mathbf{u}^* = \frac{\mathbf{u} T_0}{L_0}, \quad t^* = \frac{t}{T_0}, \quad m^* = \frac{m}{M_0}, \quad \mu^* = \mu L_0, \quad (2.7)$$

s	a_1	a_2	a_3	c_1	c_2
1	5.346773	0.004878	0.385549	0.005	0.995
2	4.688895	0.009581	0.511605	0.01	0.99
3	4.314010	0.014143	0.625785	0.015	0.985

TABLE 1. Table of values for s , a_1 , a_2 , a_3 and x_{\min} .

where M_0 is a characteristic mobility. We note that the concentration c and $W'(c)$ are dimensionless quantities. The dimensionless system takes the form

$$\partial_t^* c + \operatorname{div}^*(c\mathbf{v}^*) - \frac{1}{\mathbb{P}\mathfrak{e}} \operatorname{div}^*(m^* \nabla^* \mu^*) = 0, \quad (2.8a)$$

$$\mu^* - \mathbb{C}\mathfrak{n}^{-1} w(c) + \mathbb{C}\mathfrak{n} \Delta^* c = 0, \quad (2.8b)$$

$$(m^* \nabla^* \mu^*) \cdot \mathbf{n} = 0, \quad (2.8c)$$

$$\nabla^* c \cdot \mathbf{n} = 0. \quad (2.8d)$$

The dimensionless coefficients are the Cahn number $\mathbb{C}\mathfrak{n} = \varepsilon/L_0$, which expresses relative interface width, and the mobility Peclet number $\mathbb{P}\mathfrak{e} = (L_0^2)/(T_0 M_0)$, measuring the ratio of advection to diffusion. We suppress the star symbols in the remainder of this paper.

3. Numerical scheme

3.1. Spatial discretization

We choose $\mathcal{V} = H^1(\Omega)$ for the trial and weighting function spaces. The variational formulation reads

Find $(c, \mu) \in [L^2(\mathcal{T}; \mathcal{V}) \cap H^1(\mathcal{T}, L^2(\Omega))]^2$ such that for all $(v, q) \in [\mathcal{V}]^2$:

$$(v, \partial_t c)_\Omega + (v, \mathbf{v} \cdot \nabla c)_\Omega + \frac{1}{\mathbb{P}\mathfrak{e}} (\nabla v, m \nabla \mu)_\Omega = 0, \quad (3.1a)$$

$$(q, \mu)_\Omega - \mathbb{C}\mathfrak{n} (\nabla q, \nabla c)_\Omega - \frac{1}{\mathbb{C}\mathfrak{n}} (q, w(c))_\Omega = 0, \quad (3.1b)$$

where $(\cdot, \cdot)_\Omega$ is the standard $L^2(\Omega)$ inner product on the interior. Integration by parts shows that Eq. 3.1 is for smooth solutions equivalent to the strong formulation Eq. 2.8.

We apply the Bubunov-Galerkin finite element methodology to discretize in space. For this purpose, we introduce the conformal discrete space $\mathcal{V}^h \subset \mathcal{V}$ spanned by C^0 -finite element basis functions. The semi-discrete approximation of (3.1) takes the form

Find $(c^h, \mu^h) \in [L^2(\mathcal{T}; \mathcal{V}^h) \cap H^1(\mathcal{T}, L^2(\Omega))]^2$ such that for all $(v^h, q^h) \in [\mathcal{V}^h]^2$:

$$(v^h, \partial_t c^h)_\Omega + (v^h, \mathbf{v} \cdot \nabla c^h)_\Omega + \frac{1}{\mathbb{P}\mathfrak{e}} (\nabla v^h, m^h \nabla \mu^h)_\Omega = 0, \quad (3.2a)$$

$$(q^h, \mu^h)_\Omega - \mathbb{C}\mathfrak{n} (\nabla q^h, \nabla c^h)_\Omega - \frac{1}{\mathbb{C}\mathfrak{n}} (q^h, w^h)_\Omega = 0, \quad (3.2b)$$

where $c^h(0) = c_0^h$, $\mu^h(0) = \mu_0^h$, and $m^h = m(c^h)$ and $w^h = w(c^h)$ in Ω .

3.2. Temporal discretization

To introduce the time-discretization, we subdivide the time domain \mathcal{T} into elements $\mathcal{T}_n = (t_n, t_{n+1})$ of equal size $\Delta t = t_{n+1} - t_n$ with time level $n = 0, 1, \dots, N$. We adopt the conventional notation to denote the time level of a quantity with a subscript n , i.e., c_n^h and μ_n^h denote the concentration and chemical potential at time level n , respectively. The intermediate time level and time derivative of the concentration are given by

$$c_{n+1/2}^h := \frac{1}{2}(c_n^h + c_{n+1}^h), \quad \llbracket c^h \rrbracket_n := \frac{1}{\Delta t}(c_{n+1}^h - c_n^h). \quad (3.3)$$

The method in fully discrete form now reads

Given $c_n^h \in \mathcal{V}^h$, find $(c_{n+1}^h, \mu_{n+1}^h) \in [\mathcal{V}^h]^2$ such that for all $(v^h, q^h) \in [\mathcal{V}^h]^2$:

$$(v^h, \llbracket c^h \rrbracket_n)_\Omega + (v^h, \mathbf{v} \cdot \nabla c_{n+1/2}^h)_\Omega + \frac{1}{\mathbb{P}e} (\nabla v^h, m(c_{n+1/2}^h) \nabla \mu_{n+1}^h)_\Omega = 0, \quad (3.4a)$$

$$(q^h, \mu_{n+1}^h)_\Omega - \mathbb{C}n (\nabla q^h, \nabla c_{n+1/2}^h)_\Omega - \frac{1}{\mathbb{C}n} (q^h, w_{n+1/2}^h)_\Omega = 0. \quad (3.4b)$$

The definition of $w_{n+1/2}^h$ depends on the free energy functional. For the GL Helmholtz free energy $W(c) = G(c)$, we take $w_{n+1/2}^h = w(c_{n+1/2}^h)$, and for the FH free energy $W(c) = F(c)$, we select the first-order approximation

$$w_{n+1/2}^h = a_3 \left(\log(c_n^h) - \log(1 - c_n^h) + a_1(1 - 2c_n^h) + (\lambda + 1) \left(\frac{c_{n+1}^h}{c_n^h} - \frac{1 - c_{n+1}^h}{1 - c_n^h} \right) \right), \quad (3.5)$$

where λ is a positive numerical parameter. The definition given in Eq. 3.5 coincides with the discretization of the chemical potential of the Allen-Cahn equation of Wang *et al.* (2020). Their scheme ensures bound preservation for the Allen-Cahn equation and is constructed to guarantee energy stability. The latter is inherited from the CH equation (without advection). In particular, we have

$$F(c_{n+1}^h) - F(c_n^h) \leq w_{n+1/2}^h (c_{n+1}^h - c_n^h). \quad (3.6)$$

4. Numerical experiments

4.1. Problem setup

We use the two-dimensional swirl benchmark problem (Bell *et al.* 1989) to compare the boundedness and Ostwald-ripening properties of the advective CH equation of both free energy functionals. A circle with $c \approx 1$ and initial radius $R_0 = 0.15$ is placed in the square domain $[0, 1]^2 \subset \Omega$ at location $(x^*, y^*) = (0.35, 0.35)$ with concentration field $c \approx 0$. The circle is stretched out due to the divergence-free velocity field given by

$$\mathbf{v} = A(t)(\sin(2\pi y) \sin(\pi x) \sin(\pi x), -\sin(2\pi x) \sin(\pi y) \sin(\pi y)), \quad (4.1)$$

where $A = A(t) = \cos(\pi t/8)$ provides a periodic motion in $\mathcal{T} = (0, T)$ with $T = 8$. This causes the circle to stretch out for $0 < t < 4$ and contract for $4 < t < T = 8$. For small $\mathbb{C}n$ and large $\mathbb{P}e$ we anticipate the final configuration ($t = T$) to approximate the initial configuration ($t = 0$).

We define the initial concentration profile as

$$c_0^h(\mathbf{x}) = \frac{1}{2} \left(1 - c_r \tanh \frac{\sqrt{(x - x^*)^2 + (y - y^*)^2} - R_0}{\mathbb{C}n\sqrt{2}} \right), \quad (4.2)$$

so that $c_0^h \approx c_1$ outside the circle, and $c_0^h \approx c_2$ inside of it. For the GL potential, we set $c_r = 1$, and for the FH potential, we choose the parameters of $s = 2$ leading to $c_r = 0.98$ and $\lambda = 2$. We first solve the CH equation without advection until a stable configuration is reached. We use this concentration field as the initial configuration for the advective CH simulations. All our simulations are performed in FEniCS and utilize linear triangular finite elements for both the concentration and the chemical potential (Logg *et al.* 2012). We use as mesh width $h = 1/256$, and set $\Delta t = 4 \times 10^{-3}$ so that the Courant-Friedrichs-Lewy (CFL) number approximately equals 1. We select a relatively large interface width parameter of $\text{Cn} = 4h$ to realize the breakup of the stretched circle and take $\text{Pe} = 8/(3\text{Cn}^2)$.

We visualize the evolution of the concentration field for GL and FH potentials in Figure 3. In both simulations, the circle breaks up, and smaller circles are formed. The key difference between the two simulations is that the small circles vanish for the GL potential but persist for the FH potential. We observe the boundedness property of the FH simulation. In contrast, the GL setup violates bounds; it yields overshoots of more than 2%. The breakup of the filament (which is purely numerical) is delayed in the case of FH and the filament maintains its shape longer compared to the GL case. This delayed breakup is a useful property, as any breakup in this configuration is purely numerical (because of the absence of surface tension in 2D), and prevention and minimization of the numerical breakup of a method for a given mesh resolution is desirable.

Both simulations reasonably recover the initial profile. The recovery depends on the interface thickness parameter and mesh resolution. A detailed convergence analysis of shape recovery as a function of these factors is a future research direction.

5. Conclusions and outlook

In this paper we have compared Ostwald-ripening phenomena within the context of Cahn-Hilliard dynamics using numerical simulations. We have adopted two free energy functionals, the Ginzburg-Landau and the Flory-Huggins potentials. To enable large time-step simulations with the latter, we have proposed a novel numerical scheme. Our simulations demonstrate that adopting the Ginzburg-Landau potential violates the physical bounds and shows Ostwald ripening. In contrast, using the Flory-Huggins potential provides a bound-preserving simulation free of Ostwald ripening. Potential future research directions include (i) a detailed convergence analysis and comparison of the Flory-Huggins case with the Ginzburg-Landau case; (ii) energy-stable and bound-preserving discretizations for a Flory-Huggins Navier-Stokes Cahn-Hilliard model; (iii) the extension of the study on Ostwald ripening to high-Reynolds number multiphase flows (see, e.g., Saurabh *et al.* (2023)), N-phase flows (see, e.g., Huang *et al.* (2020); ten Eikelder (2024)), and mixture models (see e.g. Abels (2024); ten Eikelder *et al.* (2024)), leveraging energy-stable schemes to ensure robust and accurate simulations.

Acknowledgments

The authors thank S. Mirjalili, Z. Huang and L.J. Brown for helpful discussions.

REFERENCES

- ABELS, H. 2024 Mixture theory for diffuse interface models of two-phase flows. *J. Fluid Mech.* **992**, F1.

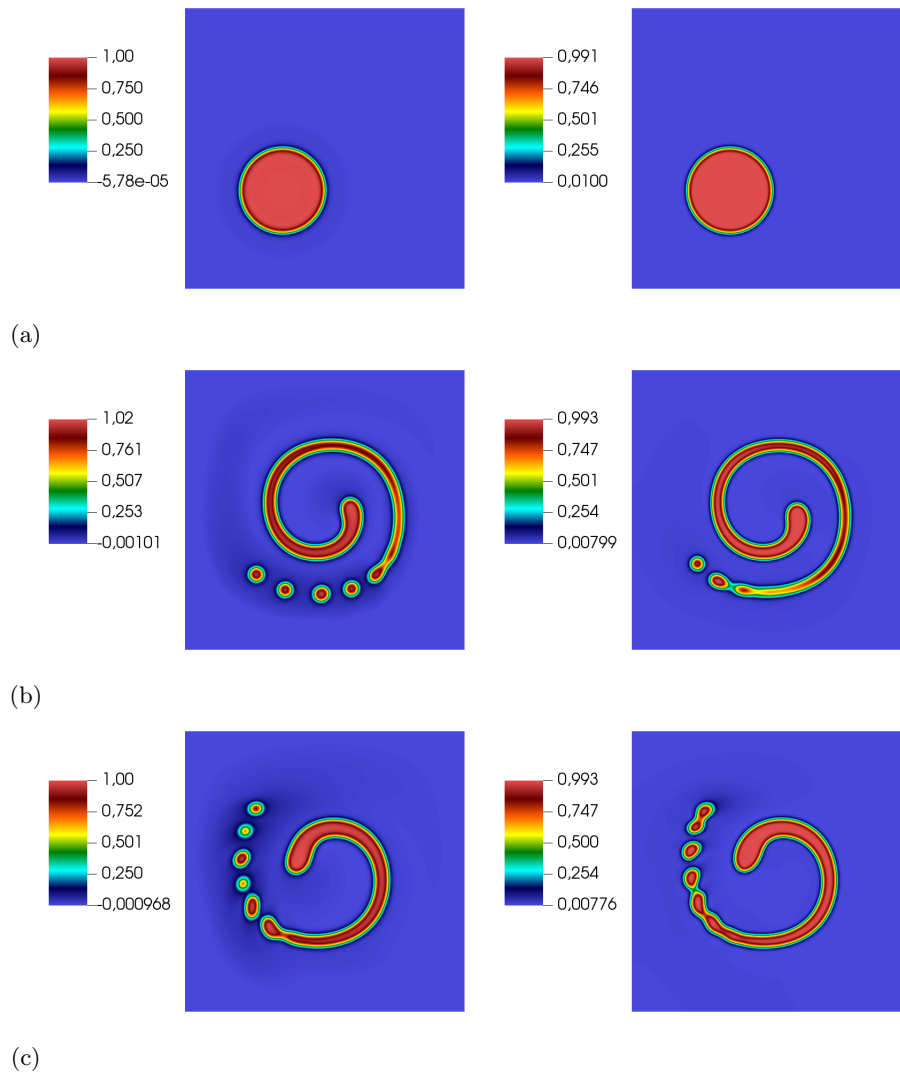
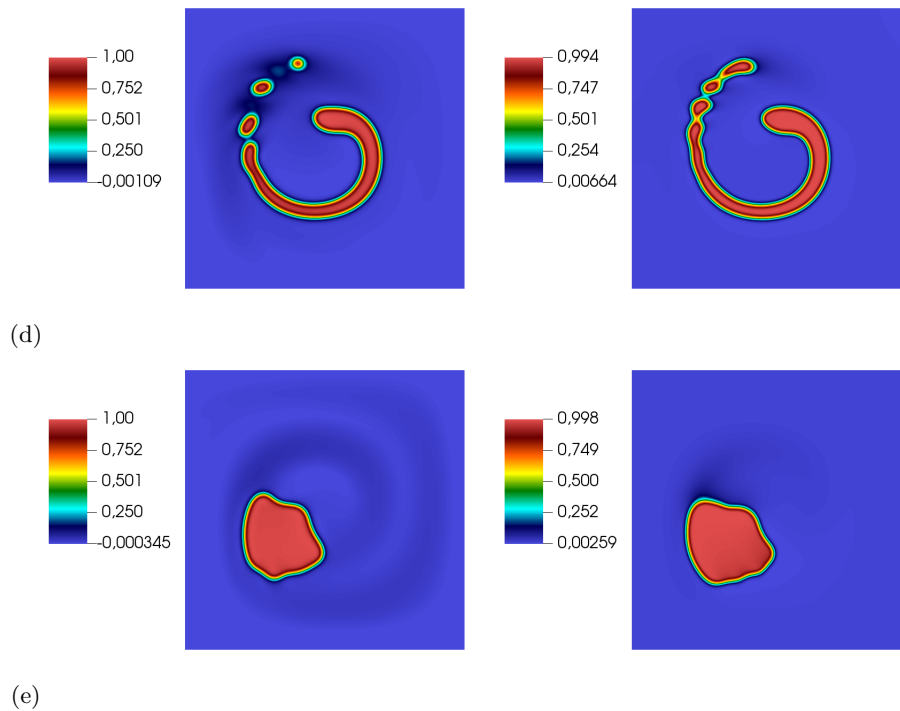


FIGURE 3. Swirl problem. GL (left) and FH potential (right). (a) $t = 0.0$, (b) $t = 4.0$, (c) $t = 5.76$. Cont'd on next page.

- ABELS, H., GARCKE, H. & GRÜN, G. 2012 Thermodynamically consistent, frame indifferent diffuse interface models for incompressible two-phase flows with different densities. *Math. Mod. Meth. Appl. S.* **22**, 1150013.
- ANDERSON, D., MCFADDEN, G. & WHEELER, A. 1998 Diffuse-interface methods in fluid mechanics. *Annu. Rev. Fluid Mech.* **30**, 139–165.
- BARRETT, J., BLOWEY, J. & GARCKE, H. 1999 Finite element approximation of the Cahn–Hilliard equation with degenerate mobility. *SIAM J. Numer. Anal.* **37**, 286–318.
- BELL, J. B., COLELLA, P. & GLAZ, H. M. 1989 A second-order projection method for the incompressible navier-stokes equations. *J. Comput. Phys.* **85**, 257–283.

FIGURE 3. Cont'd (d) $t = 6.08$, (e) $t = 8.0$.

- CAHN, J. & HILLIARD, J. 1958 Free energy of a nonuniform system. i. interfacial free energy. *J. Chem. Phys.* **28**, 258–267.
- CHEN, W., JING, J., LIU, Q., WANG, C. & WANG, X. 2024 A second order numerical scheme of the Cahn-Hilliard-navier-stokes system with Flory-Huggins potential. *Communications in Computational Physics* **35** (3), 633–661.
- DAI, S. & DU, Q. 2016 Computational studies of coarsening rates for the Cahn-Hilliard equation with phase-dependent diffusion mobility. *J. Comput. Phys.* **310**, 85–108.
- TEN EIKELDER, M. F. P. 2024 A unified framework for N -phase Navier-Stokes Cahn-Hilliard Allen-Cahn mixture models with non-matching densities. *arXiv preprint: 2407.20145*.
- TEN EIKELDER, M. F. P. & SCHILLINGER, D. 2024 The divergence-free velocity formulation of the consistent Navier-Stokes Cahn-Hilliard model with non-matching densities, divergence-conforming discretization, and benchmarks. *J. Comput. Phys.* p. 113148.
- TEN EIKELDER, M. F. P., VAN DER ZEE, G., K. & SCHILLINGER, D. 2024 Thermodynamically consistent diffuse-interface mixture models of incompressible multicomponent fluids. *J. Fluid Mech.* **990**, A8.
- TEN EIKELDER, M. F. P., VAN DER ZEE, K. G., AKKERMAN, I. & SCHILLINGER, D. 2023 A unified framework for Navier-Stokes Cahn-Hilliard models with non-matching densities. *Math. Mod. Meth. Appl. S.* **33**, 175–221.
- ELLIOTT, C. & GARCKE, H. 1996 On the Cahn-Hilliard equation with degenerate mobility. *Siam journal on mathematical analysis* **27**, 404–423.

- FLORY, P. 1953 *Principles of Polymer Chemistry*. Cornell University Press.
- GINZBURG, V. & LANDAU, L. 1950 *On the theory of superconductivity*. Berlin: Springer Nature.
- GOMEZ, H. & VAN DER ZEE, K. 2018 Computational phase-field modeling. *Encycl. of Comput. Mech. 2nd ed.* (eds. E. Stein, R. de Borst & T.J.R. Hughes) pp. 1–35.
- GUO, Z., CHENG, Q., LIN, P., LIU, C. & LOWENGRUB, J. 2022 Second order approximation for a quasi-incompressible Navier-Stokes Cahn-Hilliard system of two-phase flows with variable density. *J. Comput. Phys.* **448**, 110727.
- HUANG, Z., LIN, G. & ARDEKANI, A. M. 2020 Consistent and conservative scheme for incompressible two-phase flows using the conservative Allen-Cahn model. *J. Comput. Phys.* **420**, 109718.
- KHANWALE, M., LOFQUIST, A., SUNDAR, H., ROSSMANITH, J. & GANAPATHYSUBRAMANIAN, B. 2020 Simulating two-phase flows with thermodynamically consistent energy stable Cahn-Hilliard Navier-Stokes equations on parallel adaptive octree based meshes. *J. Comput. Phys.* **419**, 109674.
- KHANWALE, M., SAURABH, K., FERNANDO, M., CALO, V., SUNDAR, H., ROSSMANITH, J. & GANAPATHYSUBRAMANIAN, B. 2022a A fully-coupled framework for solving Cahn-Hilliard Navier-Stokes equations: Second-order, energy-stable numerical methods on adaptive octree based meshes. *Comput. Phys. Commun.* **280**, 108501.
- KHANWALE, M. A., SAURABH, K., ISHII, M., SUNDAR, H. & GANAPATHYSUBRAMANIAN, B. 2022b Breakup dynamics in primary jet atomization using mesh- and interface-refined Cahn-Hilliard Navier-Stokes. *arXiv preprint: 2209.13142* .
- LOGG, A., MARDAL, K.-A. & WELLS, G. 2012 *Automated Solution of Differential Equations by the Finite Element Method: The FEniCS book, Lect. Notes Sci. Comput. Eng.*, vol. 84. Springer-Verlag.
- LOWENGRUB, J. & TRUSKINOVSKY, L. 1998 Quasi-incompressible Cahn-Hilliard fluids and topological transitions. *Proc. R. Soc. of London A* **454**, 2617–2654.
- MIRJALILI, S., IVEY, C. B. & MANI, A. 2020 A conservative diffuse interface method for two-phase flows with provable boundedness properties. *J. Comput. Phys.* **401**, 109006.
- ROCCON, A., ZONTA, F. & SOLDATI, A. 2023 Phase-field modeling of complex interface dynamics in drop-laden turbulence. *Phys. Rev. Fluids* **8**, 090501.
- SAURABH, K., ISHII, M., KHANWALE, M., SUNDAR, H. & GANAPATHYSUBRAMANIAN, B. 2023 Scalable adaptive algorithms for next-generation multiphase flow simulations. In *2023 IEEE Int. Parallel Distrib. Process. Symp. (IPDPS)*, pp. 590–601. IEEE.
- VOORHEES, P. 1985 The theory of Ostwald ripening. *J. Stat. Phys.* **38** (1), 231–252.
- WANG, X., KOU, J. & CAI, J. 2020 Stabilized energy factorization approach for Allen-Cahn equation with logarithmic Flory-Huggins potential. *J. Sci. Comput.* **82** (2), 25.
- YUE, P., ZHOU, C. & FENG, J. J. 2007 Spontaneous shrinkage of drops and mass conservation in phase-field simulations. *J. Comput. Phys.* **223**, 1–9.